The EMBO Journal (2011) 30, 1593–1607 | © 2011 European Molecular Biology Organization | All Rights Reserved 0261-4189/11
www.embojournal.org

THE EMBO JOURNAL

Endocytosis of EphA receptors is essential for the proper development of the retinocollicular topographic map

Sooyeon Yoo[1], Yujin Kim[1], Hyuna Noh, Haeryung Lee, Eunjeong Park and Soochul Park*

Department of Biological Science, Sookmyung Women's University, Chungpa-Dong 2-Ka, Yongsan-Ku, Seoul, Korea

Endocytosis of Eph–ephrin complexes may be an important mechanism for converting cell–cell adhesion to a repulsive interaction. Here, we show that an endocytosis-defective EphA8 mutant forms a complex with EphAs and blocks their endocytosis in cultured cells. Further, we used bacterial artificial chromosome transgenic (Tg) mice to recapitulate the anterior > posterior gradient of *EphA* in the superior colliculus (SC). In mice expressing the endocytosis-defective EphA8 mutant, the nasal axons were aberrantly shifted to the anterior SC. In contrast, in Tg mice expressing wild-type EphA8, the nasal axons were shifted to the posterior SC, as predicted for the enhanced repellent effect of ephrinA reverse signalling. Importantly, Rac signalling was shown to be essential for EphA–ephrinA internalization and the subsequent nasal axonal repulsion in the SC. These results indicate that endocytosis of the Eph–ephrin complex is a key mechanism by which axonal repulsion is generated for proper guidance and topographic mapping.

The EMBO Journal (2011) **30,** 1593–1607. doi:10.1038/emboj.2011.44; Published online 22 February 2011
Subject Categories: signal transduction; neuroscience
Keywords: endocytosis; EphA; ephrinA; retinocollicular topographic map

Introduction

Eph receptor tyrosine kinases and their ligands, the ephrins, are not only the key players in axonal pathfinding during neural development but also modulate synapse formation and neuronal plasticity in the adult (Flanagan and Vanderhaeghen, 1998; Wilkinson, 2001; Kullander and Klein, 2002; Yamaguchi and Pasquale, 2004; Klein, 2009). More recent findings demonstrate that Eph receptors and ephrins coordinate physiological processes and homeostasis of diverse adult organs (Pasquale, 2005, 2008). These emerging Eph–ephrin functions suggest that the unbalanced signalling of these molecules may lead to the genesis of a variety of diseases, such as diabetes and cancer (Batlle *et al*, 2005; Konstantinova *et al*, 2007). An intriguing feature of Eph–ephrin signalling is that Ephs and ephrins elicit bidirectional signalling between two opposing cells that is contact-dependent because both molecules are membrane attached (Holland *et al*, 1996; Bruckner and Klein, 1998; Knoll and Drescher, 2002). In this system, the signal is simultaneously transduced in both ligand- (reverse signalling) and receptor-expressing cells (forward signalling). Because ephrinBs are transmembrane proteins, reverse signalling by ephrinBs is initiated through association of their short intracellular domain with other intracellular signalling proteins (Cowan and Henkemeyer, 2001; Segura *et al*, 2007; Xu and Henkemeyer, 2009). Unlike ephrinBs, ephrinAs do not possess an intracellular domain. Nevertheless, they are tethered to the plasma membrane through a GPI linkage and are capable of triggering the activation of intracellular signalling pathways through association with transmembrane proteins. Examples of transmembrane protein partners for ephrinAs include the TrkB receptor and p75 neurotrophin receptor (NTR; Lim *et al*, 2008; Marler *et al*, 2008).

Reverse signalling by ephrinAs has recently emerged as a key mechanism regulating axon guidance and topographic mapping, particularly in the well-characterized visual system from the retina to the superior colliculus (SC; Rashid *et al*, 2005; Lim *et al*, 2008). In the retinocollicular projection of rodents, the temporal (T)–nasal (N) axis of the retina topographically matches the anterior (A)–posterior (P) axis of the SC (McLaughlin and O'Leary, 2005; Flanagan, 2006). During development, EphA receptors and ephrinA ligands are expressed in opposing gradients along the T–N retinal axis as well as A–P axis of the SC. In this retina$^{\text{T–N axis}}$/SC$^{\text{A–P axis}}$ topographic mapping system, EphA–ephrinA signalling uses a contact-mediated repulsive mechanism to form the proper axonal connections. For example, in retinal ganglion cells (RGCs) of the retina, EphA receptors are expressed in a T > N gradient, whereas ephrinAs are expressed in an A < P gradient in the SC. In this EphA$^{\text{temporalRGC}}$/ephrinA$^{\text{posteriorSC}}$ module, the temporal RGC axons encounter the A < P gradient of ephrinA repellent activity in the SC, and the relative expression of the retinal EphAs determines their preferential mapping position in the anterior SC. That is, the higher the expression of EphAs is on the temporal RGC axons, the more the termination zone (TZ) is pushed towards the anterior SC. In this system, EphA forward signalling likely mediates the repellent behaviour of the temporal RGC axons (Feldheim *et al*, 2004). On the other hand, a second repellent activity with a gradient opposing the ephrinA gradient in the SC is implicated in the correct mapping of the nasal RGC axons to the posterior SC (Reber *et al*, 2004; Rashid *et al*, 2005). For example, ephrinA ligands are expressed in a T < N gradient in the RGC axons, whereas EphA

*Corresponding author. Department of Biological Science, Sookmyung Women's University, Chungpa-Dong 2-Ka, Yongsan-Ku, Seoul 140-742, Korea. Tel.: +822 710 9330; Fax: +822 715 9331;
E-mail: scpark@sookmyung.ac.kr
[1]These authors contributed equally to this work

Received: 17 October 2010; accepted: 28 January 2011; published online: 22 February 2011

receptors are expressed in A>P gradient in the SC. In this ephrinA^{nasalRGC}/EphA^{anteriorSC} system, the nasal RGC axons are repelled by EphAs in the anterior SC due to the ephrinA^{retina}–EphA^{SC} repulsive interactions, and therefore, their appropriate mapping in the posterior SC is determined by the relative expression of ephrinAs on the nasal RGC axons. In this system, EphA receptors in the anterior SC act as corresponding ligands on the retinal axons, in which ephrinAs act as receptors, and therefore trigger reverse signalling through their associated signalling components. Consistent with this hypothesis, topographic mapping of nasal axons is disrupted in mutant mice null for *EphA7*, which is expressed in an A>P gradient in the SC but is not expressed in the retina (Rashid *et al*, 2005). In addition, a recent study shows that p75^{NTR} is a component of signalling induced by ephrinAs present on the nasal RGC axons and that its genetic deletion results in aberrant mapping of the nasal RGC axons in the SC (Lim *et al*, 2008). Therefore, the opposing gradient and repellent activities of EphAs and ephrinAs in the SC likely have a key role in determining the topographic specificity exhibited by RGC axons along the A–P axis.

In general, Eph–ephrin interactions trigger cell–cell repulsion (Flanagan and Vanderhaeghen, 1998; Wilkinson, 2000, 2001; Pasquale, 2005). This effect is typically observed in the retina$^{T-N\ axis}$/SC$^{A-P\ axis}$ topographic mapping system. The ability of an adhesive Eph receptor–ephrin ligand interaction to generate a repellent response is paradoxical. An elegant solution to this paradox may be that the ligand–receptor complex is removed from the cell surface, thereby converting adhesive events into repulsive events. Two mechanisms supporting this idea have been reported: proteolytic shedding of the ephrin ectodomain following Eph engagement (Hattori *et al*, 2000; Janes *et al*, 2005) and rapid endocytosis of Eph–ephrin complexes (Marston *et al*, 2003; Zimmer *et al*, 2003). Although all these reports are clearly presented and consistent, it will be of great importance to investigate whether regulation of ephrin shedding or Eph–ephrin complex internalization influences the choice between repulsion and adhesion *in vivo*, for example, in the development of the retinocollicular topographic maps.

Here, we show that the endocytosis-defective EphA8 mutant not only effectively blocks ligand-induced forward endocytosis of EphAs in SC cells but also disrupts topographic mapping of nasal RGC axons. In contrast, in transgenic (Tg) mice expressing wild-type EphA8, a converse topographic mapping defect was observed for the nasal RGC axons. Consistently, the endocytosis-defective EphA8 was an adhesive substrate for nasal RGC axon growth *in vitro*, whereas wild-type EphA8 was a repellent substrate for the nasal axons *in vitro*. These findings strongly support a model in which regulation of Eph–ephrin internalization determines the choice between repulsion and adhesion *in vivo*.

Results

Identification of a juxtamembrane region in EphA8 as the critical domain for endocytosis

Previous studies indicate that trans-endocytosis of Eph–ephrin complexes has a role in the repulsive mechanism underlying retraction of cellular processes (Marston *et al*, 2003; Zimmer *et al*, 2003). We also found that the EphA8 receptor is rapidly internalized in 293 cells in response to preclustered ephrinA5-Fc (Figure 1A). To identify the region responsible for internalization of the EphA8 receptor upon ligand binding, we used a series of EphA8 deletion mutants lacking specific intracytoplasmic regions as previously reported (Gu *et al*, 2005). Interestingly, we found that the EphA8 deletion mutant lacking the entire juxtamembrane region was not internalized in response to ephrinA5 stimulation (data not shown). As the juxtamembrane region of EphA8 is encoded by both exon 9 and exon 10, we generated smaller EphA8 deletion mutants lacking the specific region encoded by exon 9 or exon 10. The EphA8-E9 mutant lacking the exon 9-encoded peptide underwent normal endocytosis when stimulated with ephrinA5 (Figure 1A and B). In contrast, endocytosis of the EphA8-E10 mutant in response to ephrinA5 stimulation was drastically impaired (Figure 1A and B), suggesting that the exon 10-encoded peptide motif is a crucial determinant of ligand-induced endocytosis of EphA8. We also investigated whether ephrinA5 in 293 cells is internalized upon binding to its cognate Eph receptors. To investigate this reverse endocytosis, we transfected 293 cells with the ephrinA5-IRES-EGFP construct and analysed GFP-positive cells to detect the endocytosis of ephrinA5 in complex with EphA8-Fc. EphrinA5 on the cell surface was effectively bound to EphA8-Fc, but this interaction was rapidly eliminated upon acid washing (Figure 1A and B), suggesting that reverse endocytosis of ephrinA5 is not induced by EphA receptors.

To investigate whether the EphA8-E10 deletion mutant is associated with disruption of endocytosis for other EphA receptors upon ligand binding, we transfected the EphA8-IRES-EGFP construct into HEK293 cells stably expressing EphA4. Only GFP-positive cells were analysed for endocytosis of Eph–ephrin complexes as these cells show simultaneous expression of both EphA8 and EphA4 within the same cell. As expected, endocytosis of EphA receptors upon ephrinA5 binding was enhanced in cells expressing both EphA4 and EphA8 (Figure 1C and D). In contrast, in cells expressing the EphA8-E10 mutant, the endocytosis of EphA–ephrinA5 complexes was significantly impaired (Figure 1C and D). Importantly, co-immunoprecipitation studies demonstrated that both wild-type EphA8 and the EphA8-E10 mutant were able to form complexes with EphA4 in 293 cells (Figure 1E, lanes 3 and 8).

Expression of the endocytosis-defective EphA8 mutant in the SC using an EphA8-specific BAC

EphA8 is expressed in a gradient in the SC, whereas it is undetectable in the retina (Park *et al*, 1997). However, unlike *EphA7* knockout mice, *EphA8* knockout mice do not exhibit any disruption in the retinocollicular map (data not shown), possibly because of a compensatory effect by other EphA receptors. Nevertheless, we postulate that EphA8-E10 might be a useful tool for investigating whether endocytosis of EphA–ephrinA complexes is required for the formation of retinocollicular topography. For this purpose, we used *EphA8* BAC to induce stable and tissue-specific expression of the EphA8-E10 mutant *in vivo*. This *EphA8* BAC DNA has been shown to drive *LacZ* reporter gene expression specifically in the anterior region of the developing midbrain (Kim *et al*, 2007). *LacZ* expression in the same BAC Tg mice was also detected in an A>P gradient in the SC at P5 (Supplementary Figure S1). This expression

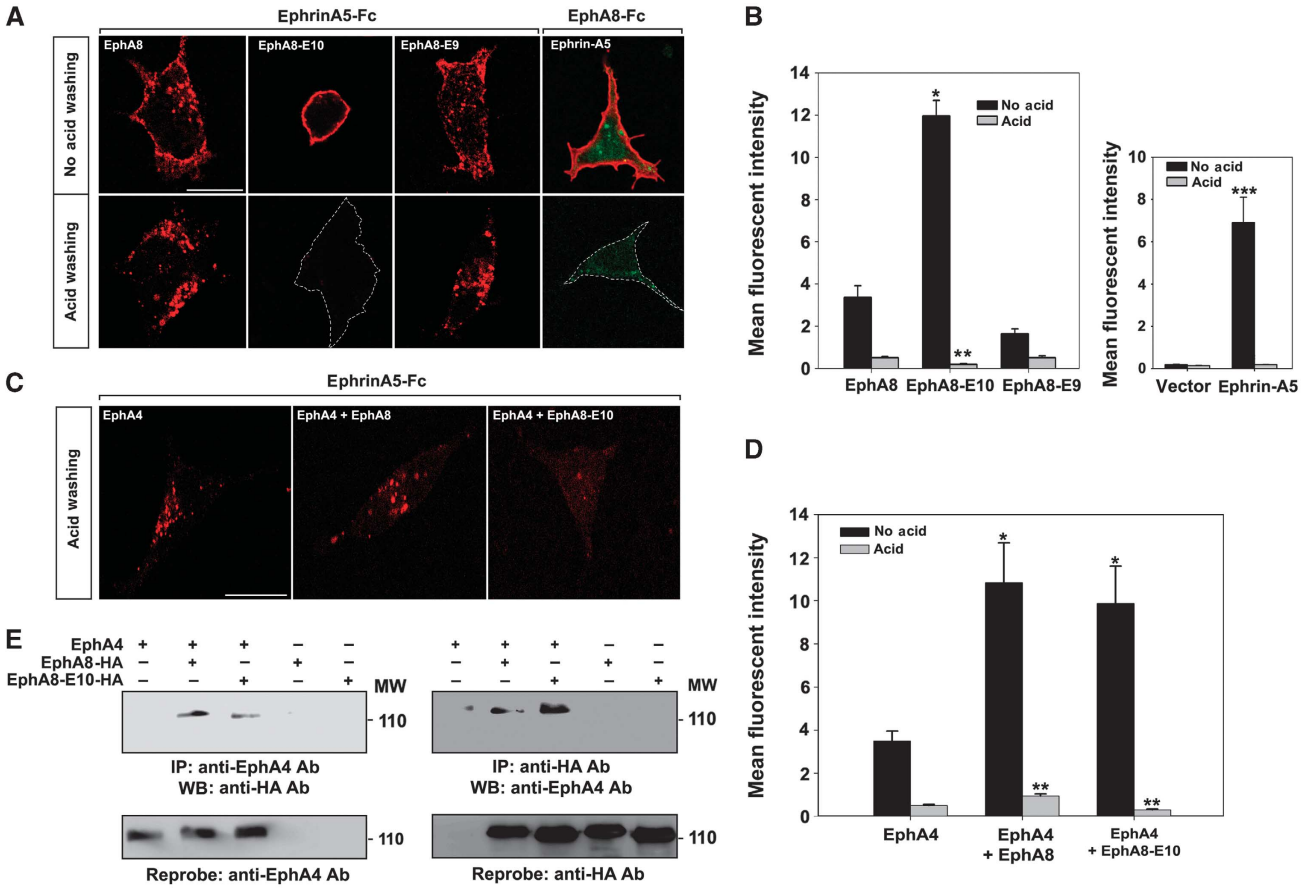

Figure 1 Identification of the EphA8 juxtamembrane region critical for ligand-induced endocytosis. (**A**) HEK293 cells stably expressing wild-type EphA8 or a EphA8 deletion mutant lacking the exon 10- or exon 9-encoded juxtamembrane region (EphA8-E10 and EphA8-E9, respectively) were stimulated with pre-clustered ephrinA5-Fc for 30 min. HEK293 cells were also transiently transfected with the ephrinA5-IRES-EGFP construct and stimulated with pre-clustered EphA8-Fc for 30 min. Cells were then fixed and permeabilized for immunostaining using a goat anti-human IgG conjugated with Texas Red dye (upper panels). To visualize internalized ephrinA5-Fc or EphA8-Fc, we washed cells with acid buffer for 10 min to remove surface-bound proteins before fixing and permeabilizing cells for immunostaining (lower panels). Scale bar = 10 μm. (**B**) The data in Figure 1A were quantitated using ImageJ software. Data represent the mean ± s.e. for at least five independent experiments, with 30 cells counted for each condition. Relative bindings of ephrinA5-Fc under different conditions were compared with that in the EphA8-transfected condition without or with acid washing (*$P<0.001$; **$P<0.01$, ANOVA). The amount of EphA8-Fc internalized into ephrinA5-expressing cells was not significantly different from that in GFP-transfected control cells (***$P<0.001$, Student's *t*-test). (**C**) HEK293 cells stably expressing EphA4 were transiently transfected with the indicated IRES-EGFP-based EphA8 expression constructs, and experiments were carried out as described in Figure 1A. Scale bar = 10 μm. (**D**) The data in Figure 1C were quantitated using ImageJ software, and only GFP-positive cells were selected for statistical analysis. Data represent the mean ± s.e. of at least five independent experiments, with 40 cells counted for each condition. Relative bindings of ephrinA5-Fc under different conditions were compared with that in the EphA4-transfected condition without or with acid washing (*$P<0.001$; **$P<0.01$, ANOVA). (**E**) Cell lysates were subjected to immunoprecipitation (IP) using anti-EphA4 antibodies (Ab; left) or anti-HA Ab (right), and immune complexes were analysed by western blot (WB) using the indicated Ab (top panels). The blots were reprobed to determine the level of EphA4 or HA-tagged EphA8 proteins (bottom panels).

pattern remained unchanged until P8 and was barely detectable after P10 (data not shown). This expression pattern is consistent with that of the endogenous *EphA8* gene, as determined using *EphA8*$^{lacZ/lacZ}$ mice.

The *EphA8* gene contains 17 exons and is positioned approximately in the centre of the *EphA8* BAC clone, RP23-357K18, as described (Kim *et al*, 2007). To generate the recombinant *EphA8* BAC-expressing EphA8-E10 mutant, we selectively eliminated exon 10 by homologous recombination in a bacterial system (Supplementary Figure S1C). The final *EphA8* BAC clone was injected into a fertilized ICR mouse zygote to generate BAC Tg mice expressing the EphA8-E10 mutant. Both RT–PCR and western blot analysis of SC extracts from P5 mice revealed that EphA8-E10 was stably expressed in two different Tg mice (Supplementary Figure S1D and E). Furthermore, RNA *in situ* hybridization analysis of EphA family members revealed that *EphA4*, *EphA7* and *EphA8* were expressed more strongly in the anterior part of the SC, while ephrinA5 was expressed at higher levels in the posterior part of the SC (Supplementary Figure S2A). Their expression patterns were not significantly altered between wild-type and Tg mice expressing the EphA8-E10 mutant. In addition, we used ephrinA5-Fc and EphA8-Fc affinity probes to detect the overall distribution of EphA receptors and ephrinA ligands in the SC at P2, respectively (Supplementary Figure S2B). In both wild-type and EphA8-E10 Tg mice, EphAs were distributed in an overall A > P gradient in superficial layers of the SC, while ephrinAs were in an overall A < P gradient.

Aberrant retinocollicular mapping in BAC Tg mice expressing the endocytosis-defective EphA8 mutant

To explore the possible topographic disorganization of the retinocollicular projection, we introduced small focal injections of DiI in the ventronasal retina of BAC Tg mice expressing EphA8-E10 and their wild-type littermates, and then examined the contralateral SC 36 h later. All these analyses were performed using P9 mice, which have a completely mature topographic map. Ventronasal injection of DiI in wild-type mice labelled a dense, focal TZ in a topographically appropriate position in the posterior SC (Figure 2A and B). A similar ventronasal injection of DiI in BAC Tg mice expressing EphA8-E10 mutant also resulted in labelling of a dense, focal TZ in the medioposterior SC, but in about 70% of these mice, axons from the ventronasal retina formed ectopic TZs in the medioanterior part of the SC. These results were reproducibly observed in two different BAC Tg lines expressing the EphA8-E10 mutant (Figure 2C and F). Closer examination of the sagittal sections revealed that these ectopic TZs were clearly present within the SC and that the ectopic branches or arbours were positioned along the anterior–posterior position of the TZ zone (Figure 2D, E, G–I). However, temporal RGC axons in BAC Tg mice expressing the EphA8-E10 mutant did not have aberrant topographic retinocollicular projections (data not shown).

To further investigate the organization of the retinocollicular map at a population level, we developed an ephrinA5-EGFP BAC Tg line that expresses an EGFP reporter under the control of the *ephrinA5* promoter. The ephrinA5 BAC clone, RP23-23O22, contains the mouse genomic region from −6.7 kbp upstream to +214.8 kbp downstream of the ephrinA5 transcription start site (Figure 3A). The recombinant ephrinA5-EGFP BAC was generated by homologous recombination in a bacterial system in which the EGFP expression cassette was specifically inserted into the site just upstream of the ephrinA5 translational start site. This strategy selectively labelled the nasal retina, in particular, the nasal ganglion cell axons and their terminations within the SC (Figure 3B and C). The RGC axon-independent EGFP signal was also high in the posterior SC (P1–P5), consistent

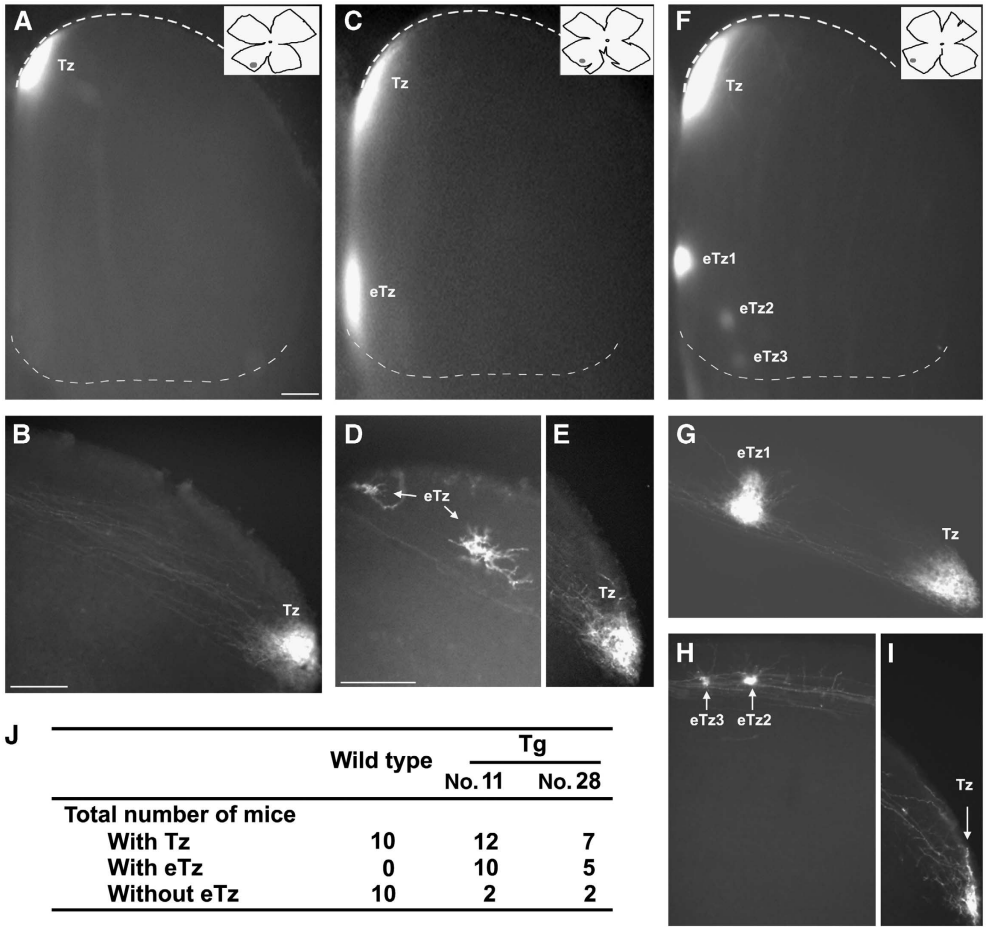

J

	Wild type	Tg	
		No. 11	No. 28
Total number of mice			
With Tz	10	12	7
With eTz	0	10	5
Without eTz	10	2	2

Figure 2 Aberrant retinocollicular mappings of nasal retinal axons in EphA8-E10 Tg mice. For anterograde tracing, P9 wild-type and EphA8-E10 Tg mice received a focal DiI injection in the ventronasal retina. After 36 h, the retina and SC were prepared, and the location of DiI in the retina and the Tz in the SC were determined. (**A**) Dorsal view of the SC in a wild-type mouse reveals a dense Tz in the posterior SC. The dotted lines mark the anterior and posterior border of the SC, respectively. Anterior is to the bottom and medial is to the left. The flat-mounted retina contralateral to the SC is shown in the smaller box, and the precise location of DiI is indicated by a dot. Nasal is to the left and dorsal is to the top. (**B**) Mid-sagittal section of the wild-type SC shown in **A**. Anterior is to the left and dorsal is to the top. (**C–E**) Analysis of the EphA8-E10 Tg line 11. Experiments were carried out as described in **A** and **B**. (**F–I**) Analysis of the EphA8-E10 Tg line 28. Experiments were carried out as described in **A** and **B**. Scale bar = 100 μm in **A**, **C** and **F** and 50 μm in **B**, **D**, **E** and **G–I**. (**J**) Statistical data revealing the topographic mapping defects in EphA8-E10 Tg mice as analysed by anterograde tracing.

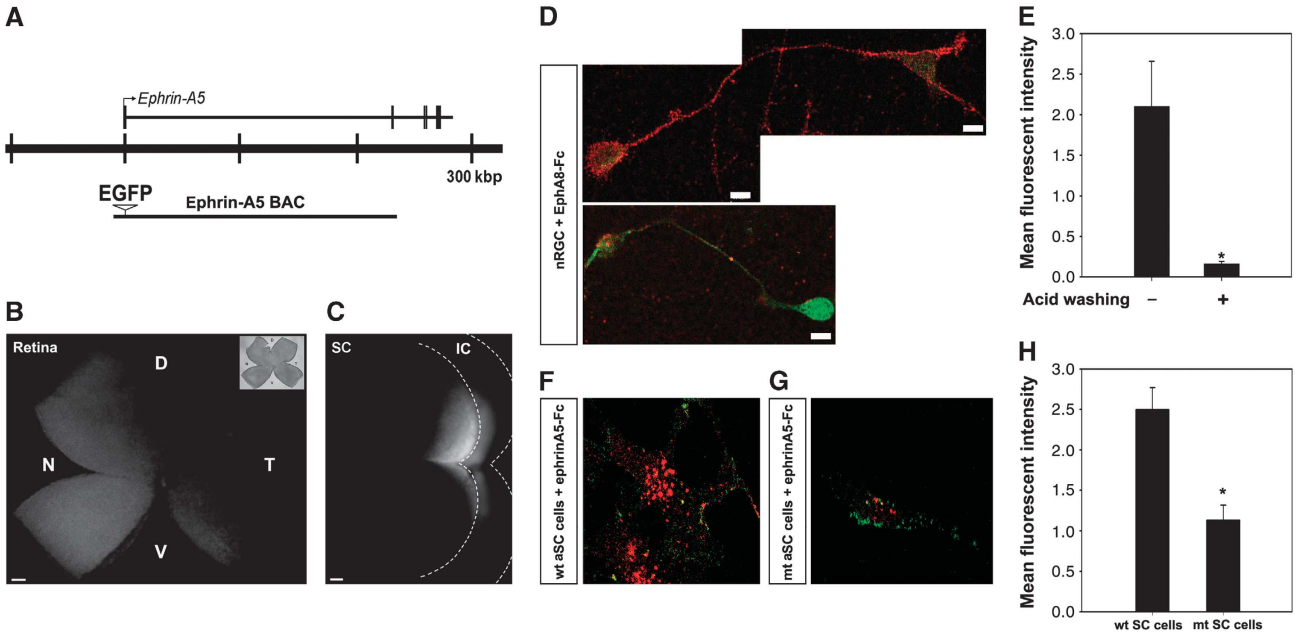

Figure 3 Endocytotic defects of EphA receptors in primary SC cells of EphA8-E10 Tg mice. (**A**) Schematic map of the ephrinA5 genomic locus with the ephrinA5 BAC clone (RP23-23O22). (**B**) GFP fluorescent image of a flat-mounted retina from an ephrinA5-EGFP BAC Tg mice at P5. D, dorsal; V, ventral. Scale bar = 200 μm. (**C**) GFP fluorescent image of a dorsal midbrain from an ephrinA5-EGFP BAC Tg mouse at P10. The GFP image was obtained 1 day after the right eye was enucleated to eliminate the contribution of EGFP-labelled RGC axon terminations to the left SC. Scale bar = 200 μm. (**D**) Analysis of reverse endocytosis of ephrinAs in nasal RGCs (nRGCs). The ventronasal retina of the ephrinA5-EGFP Tg embryo (E15) was dissected out, dissociated and cultured for 2 days. Pre-clustered EphA8-Fc proteins were treated for 30 min and stained as described in Figure 1A. Scale bar = 10 μm. (**E**) The data in Figure 3D were quantified as described in Figure 1B ($n = 40$). *$P < 0.001$, paired *t*-test. (**F**, **G**) Analysis of forward endocytosis of EphA receptors in primary SC cells. The anterior part of the SC (aSC) was dissociated from EphA8-E10 Tg embryos (E15) and their wild-type littermates. After 2 days, the cells were treated with pre-clustered ephrinA5-Fc for 30 min, fixed and incubated with FITC-conjugated anti-goat human IgG to detect cell surface-bound ephrinA5-Fc. Cells were then permeabilized, and internalized ephrinA5-Fc was stained as described in Figure 1A. (**H**) Quantitation of internalized ephrinA5-Fc in Figure 3F and G, represented by mean ± s.e. ($n = 40$). *$P < 0.001$, Student's *t*-test.

with previous findings that ephrinA5 is expressed in the SC (P > A; Frisen *et al*, 1998), but its expression was very weak at P10 as compared with the RGC axon-dependent EGFP signal (Figure 3C). To analyse the endocytotic ability of ephrinA or EphA *in vivo*, EGFP-labelled RGCs were prepared from the nasal retina of the ephrinA5-EGFP Tg embryo at embryonic day 15 (E15), and we then assessed whether treatment of EphA8-Fc elicits reverse endocytosis through ephrinA5. As expected, EphA8-Fc was bound only to GFP-positive ganglion cells with the longer axons, but upon acid washing, EphA8-Fc binding was effectively abolished, consistent with our data in 293 cells (Figure 3D and E). In contrast, experiments using anterior SC cells prepared from wild-type embryos at E15 revealed that EphA receptors were rapidly internalized in response to ephrinA5-Fc treatment (Figure 3F). In addition, anterior SC cells from the BAC Tg embryo expressing the EphA8-E10 mutant exhibited at least a two-fold reduction in the endocytotic ability of EphA receptors in response to ephrinA5 treatment, supporting the dominant negative function of EphA8-E10 (Figure 3G and H).

Next, we crossed the ephrinA5-EGFP line with EphA8-E10 BAC Tg mice to more broadly investigate the effect of the endocytosis-defective EphA8 mutant on retinotopic mapping. In ephrinA5-EGFP mice without EphA8-E10, the projection of EGFP-labelled nasal RGC axons revealed the specific retinotopic pattern of axon terminations in the posterior SC (Figure 4A and B). However, in the compound Tg lines expressing both EGFP and EphA8-E10, the termination pattern formed by EGFP-labelled nasal RGC axons showed a significant anterior expansion in the posterior SC. These results were reproducibly observed in two different Tg lines expressing the EphA8-E10 mutant (Figure 4A and B). The effect of the endocytosis-defective EphA8 mutant on the retinotopic pattern of EGFP-labelled nasal RGC axons was more prominent in the TG-28 line. In this Tg line, the EGFP-positive termination domain in the most anterior border was often separated from the rest of the nasal retinotopic domain. Parasagittal sections across the SC in these compound Tg animals provided more clear evidence that the terminations of nasal RGC axons in the SC were expanded anteriorly in EphA8-E10 BAC Tg mice (Figure 4A and B, panels a–f). To quantify the mapping changes, we measured the most anterior border of the EGFP-positive area in the SC. Compared with wild-type littermates, EphA8-E10 Tg mice had an anterior-most border that was anteriorly shifted, particularly in the medioposterior SC (Figure 4A and B, third panels).

Converse mapping defects in BAC Tg mice expressing the wild-type EphA8 receptor

To further investigate the effect of wild-type EphA8 on retinotopic mapping *in vivo*, we injected the *EphA8* BAC clone directly into a fertilized ICR mouse zygote to generate BAC Tg mice overexpressing the wild-type EphA8 receptor. Both RT–PCR and western blot analyses of SC extracts showed that an approximate two-fold increase in wild-type EphA8 expression occurred (Figure 5D). Next, we crossed the

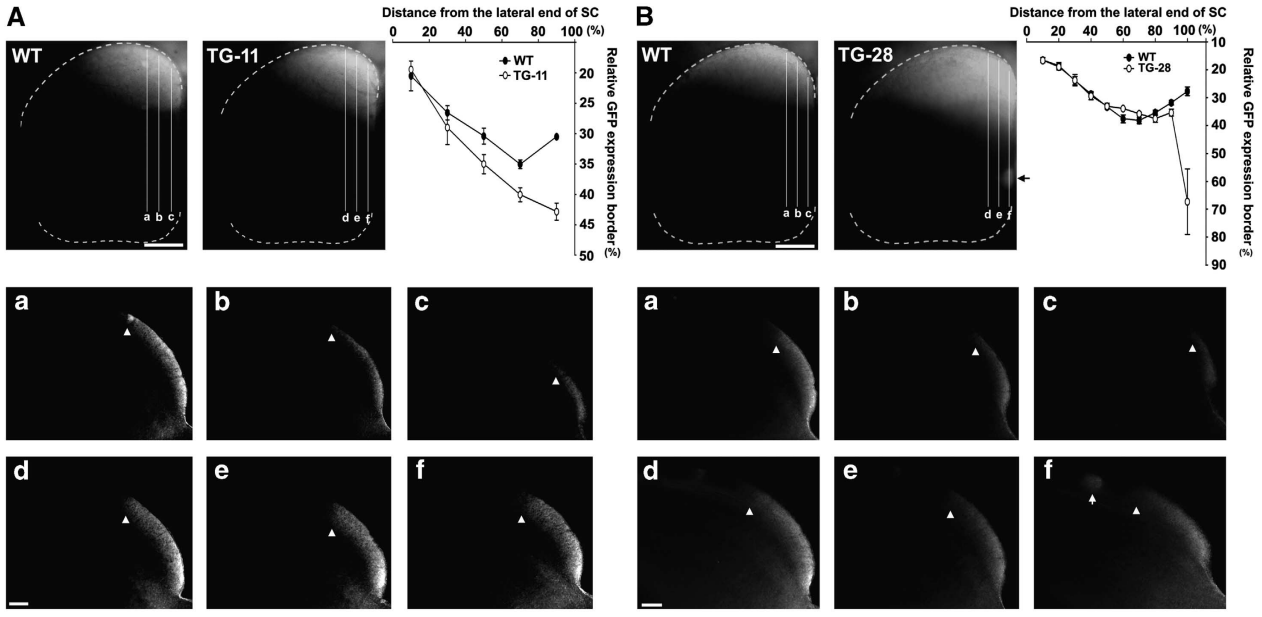

Figure 4 Topographic mapping analysis of EGFP-labelled nasal RGC axons in ephrinA5-EGFP; EphA8-E10 compound Tg mice. (**A**) The ephrinA5-EGFP line was crossed with the EphA8-E10 BAC Tg line 11, and their P9 littermates were examined for retinotopic mapping as described in Figure 3C. For each Tg line, the average position of the anterior border of the EGFP-labelled axon terminations from the posterior end of the SC was measured and expressed as a percentage of the anterior–posterior extent of the SC (top and third panel). Statistical data represent the mean (±s.e.) of 12–14 cases for each line. Corresponding sections from the SC of WT and TG-11 are shown in panels a–f. An arrowhead marks the anterior border of each EGFP-labelled termination domain. Scale bar = 400 μm. (**B**) Experiments were carried out essentially as described in **A**, except that the ephrinA5-EGFP line was crossed with EphA8-E10 BAC Tg line 28. Arrows indicate ectopic termination domains separated from the rest of the nasal retinotopic domain. Statistical data represent the mean (±s.e.) of 10 to 12 cases for each line. Scale bar = 400 μm.

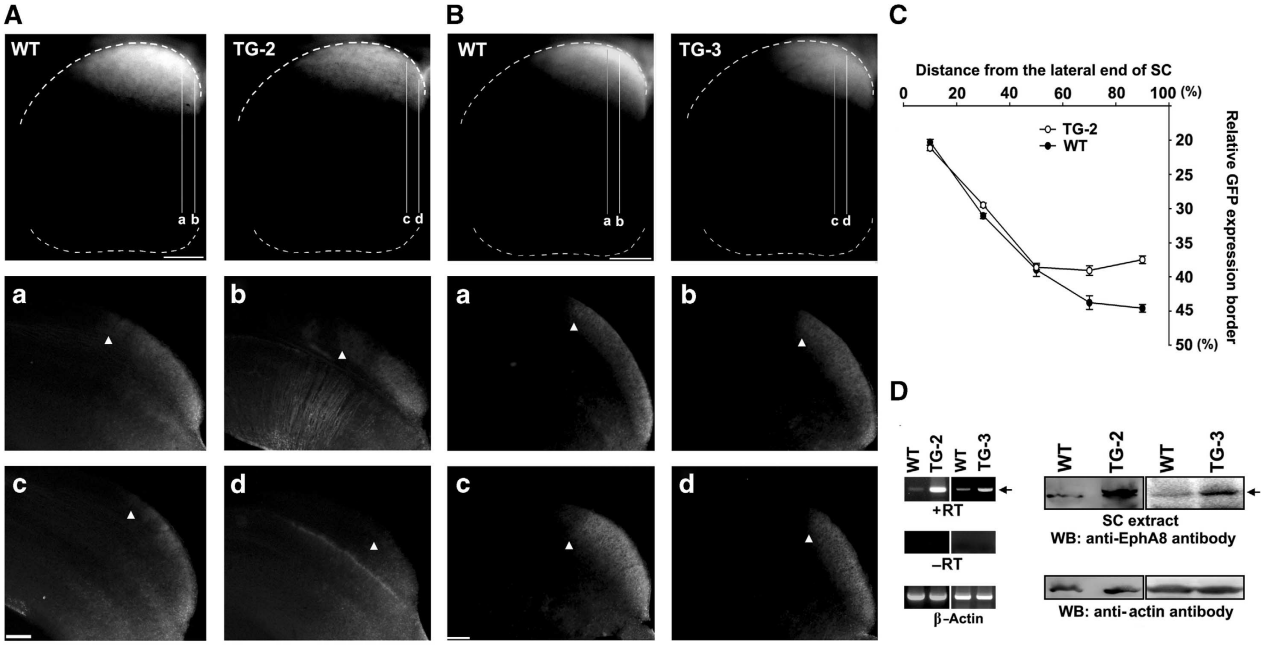

Figure 5 Topographic mapping analysis of EGFP-labelled nasal RGC axons in ephrinA5-EGFP; EphA8 compound Tg mice. The ephrinA5-EGFP line was crossed with the EphA8 BAC Tg line, and their P9 littermates were examined for retinotopic mapping as described in Figure 4. EphA8 BAC Tg lines were generated by injecting the EphA8 BAC DNA (unmodified version of the RP23-357K18 clone). (**A**, **B**) Sagittal sections corresponding to the lines present in the SC of each Tg line are shown in panels a–d. An arrowhead marks the anterior border of each EGFP-labelled termination domain. Scale bar = 400 μm. (**C**) Plot illustrating the average position of the anterior border of the EGFP-labelled axon terminations, expressed as a percentage of the anterior–posterior extent of the SC in WT or TG-2 Tg mice as described in Figure 4. Statistical data represent the mean ± s.e. ($n = 9$/each line). (**D**) Expression analysis using RT–PCR (left panels) or western blot (WB).

EphA8 BAC Tg lines with ephrinA5-EGFP mice to generate the compound mice, which express wild-type EphA8 in the anterior SC as well as EGFP under the control of the *ephrinA5* promoter. In contrast to wild-type littermates, which showed a normal distribution of EGFP-positive nasal RGC axon terminations, the compound Tg lines exhibited altered

retinotopic mapping. Specifically, the termination domains were reduced in size and posteriorly shifted in the SC (Figure 5A and B). This altered pattern of the EGFP-labelled termination domain in the posterior SC was confirmed by examining parasagittal sections across the SC of each mouse (Figure 5A and B, panels a–d). We also measured the most anterior border of the EGFP-positive area in the SC to quantify the mapping alterations between wild-type and EphA8-expressing mice. The most anterior border of EGFP-positive termination domains was more posteriorly shifted in EphA8-expressing Tg mice than in wild-type littermates, and this altered pattern was more evident in the medioposterior SC (Figure 5C). Consistent with these results, focal injections of DiI in nasal retina of EphA8-expressing BAC Tg mice revealed that the TZ shifted posteriorly at P9, an opposite result from what we observed in EphA8-E10 Tg mice (data not shown).

The endocytosis-defective EphA8 mutant attracts nasal RGC axons in in vitro explant culture

To better understand the mechanism responsible for the different retinotopic mapping in the presence of wild-type EphA8 or EphA8-E10, we developed a co-culture system consisting of both a mouse E14.5 retina explant and 293 cells overexpressing EphA8 or EphA8-E10. To visualize the ephrinA5-expressing nasal RGC axons in the co-culture, we dissected out retinas from the ephrinA5-EGFP BAC Tg embryos. Similar-sized, small cell clumps were collected from 293 cell cultures, and each cell clump was placed on either side of strips of the mouse nasal retina (Figure 6A). Nasal RGC axons were allowed to grow for 2 days, and then the outgrowth preference of EGFP-positive nasal RGC axons to each of the 293 cell aggregates was measured by directly comparing the number of axons within each cell aggregate with the total number of axons extended from the explant. In our co-culture system, which gives a choice between growing on EphA8 and EphA8-E10 cell aggregates, the total number of nasal axons extending from either side of each explant was not significantly different. However, we found that nasal RGC axons demonstrated a good preference for cell aggregates expressing the EphA8-E10 mutant but a significant avoidance for cell aggregates expressing wild-type EphA8 (Figure 6A). In control experiments, temporal RGC axons did not exhibit a growth preference between EphA8 and EphA8-E10 cell aggregates (data not shown). Quantification of EGFP-positive axons revealed that a three-fold increase in growth preference occurred on EphA8-E10 mutant cell aggregates (Figure 6B).

Rac activity is required for EphA-mediated endocytosis and axonal repulsion

Our recent study showed that Tiam-1, a Rac-GEF, is poorly associated with the EphA8-E10 mutant and that Rac signalling is impaired (Yoo *et al*, 2010; see Figure 8A). More importantly, downregulation of Tiam-1 in HEK293 cells expressing EphA8 resulted in inefficient endocytosis of EphA8–ephrinA5 complexes (Supplementary Figure S3B–D). We further investigated how this downregulation of Tiam-1 affects axonal behaviour in an *in vitro* explant/cell aggregate experiment. As expected, nasal EGFP-positive RGC axons exhibited a growth preference for Tiam-1 knockdown cells despite their strong expression of EphA8, whereas they strongly avoided the same cells transfected with the mouse Tiam-1 rescue plasmid (Supplementary Figure S3E–G).

To further investigate a role of Rac signalling in endocytosis of EphA receptors, we generated several independent 293 cell lines that stably express both wild-type EphA8 and dominant-negative Rac (RacN17). As expected, these RacN17-expressing cells showed reduced Rac activity (Figure 7A and B). In addition, endocytosis of EphA8 upon ligand stimulation was drastically impaired in the RacN17-expressing cells (Figure 7C and D). When these cell aggregates were co-cultured with a mouse nasal retina explant, nasal EGFP-positive RGC axons exhibited a robust growth preference for cells expressing both EphA8 and RacN17, whereas they strongly avoided cells expressing EphA8 alone (Figure 7E). Quantification of EGFP-labelled nasal axons within the boundary of each cell aggregate revealed an approximately 2.5-fold increase in growth preference for cell aggregates expressing both EphA8 and RacN17 (Figure 7F).

Next, we assessed whether Rac activity is altered in the anterior SC of the Tg line TG-28, which expresses the EphA8-E10 mutant. As shown in Figure 8A, Rac activity in this Tg line was reduced as compared with wild-type littermates (first panel). In contrast, Rac activity was drastically enhanced in the anterior SC of the Tg line TG-2, which expresses the wild-type EphA8 receptor (second panel). To further investigate whether Rac activity has a role in regulating endocytosis of EphA receptors in the anterior SC and retinocollicular map formation, we generated BAC Tg lines that express RacN17 under the control of the EphA8 promoter. RT–PCR analysis of SC extracts showed that RacN17 is specifically expressed in the anterior SC of the Tg mice (Figure 8C). In addition, Rac activity was strongly reduced in the Tg line expressing RacN17 (Figure 8D and E). Importantly, endocytosis of EphA receptors in response to ephrinA5 stimulation was drastically impaired in SC cells isolated from the Tg line that expresses RacN17 (Figure 8F and G). Next, we crossed the ephrinA5-EGFP line with RacN17 BAC Tg mice to see the effect of RacN17 on retinotopic mapping that involves ephrinA^{nasalRGC}/EphA^{anteriorSC}. As expected, in the compound Tg lines expressing both EGFP and RacN17, the termination pattern formed by EGFP-labelled nasal RGC axons showed a significant anterior expansion in the posterior SC, similar to what we observed in Tg lines expressing EphA8-E10 (Figure 8H and I). Parasagittal sections across the SC of each mouse also confirmed this altered pattern in the EGFP-labelled termination domain (Figure 8H and I, panels a–d). Finally, quantification of the most anterior border of the EGFP-positive area in the SC also confirmed the mapping alterations between wild-type and RacN17-expressing mice (Figure 8J and K).

Discussion

The outcome of high-affinity interactions between Eph receptors and ephrins is generally cell–cell repulsion. One of the mechanisms proposed to account for this paradox is that trans-endocytosis of Eph–ephrin complexes destabilizes the cell–cell contacts and therefore, is responsible for, or at least contributes to, cell–cell repulsion (Marston *et al*, 2003; Zimmer *et al*, 2003). However, this hypothesis has been tested only in *in vitro* cultured cells, and its biological significance *in vivo* remains unclear. In the present study, we show that endocytosis of EphA receptors in the anterior

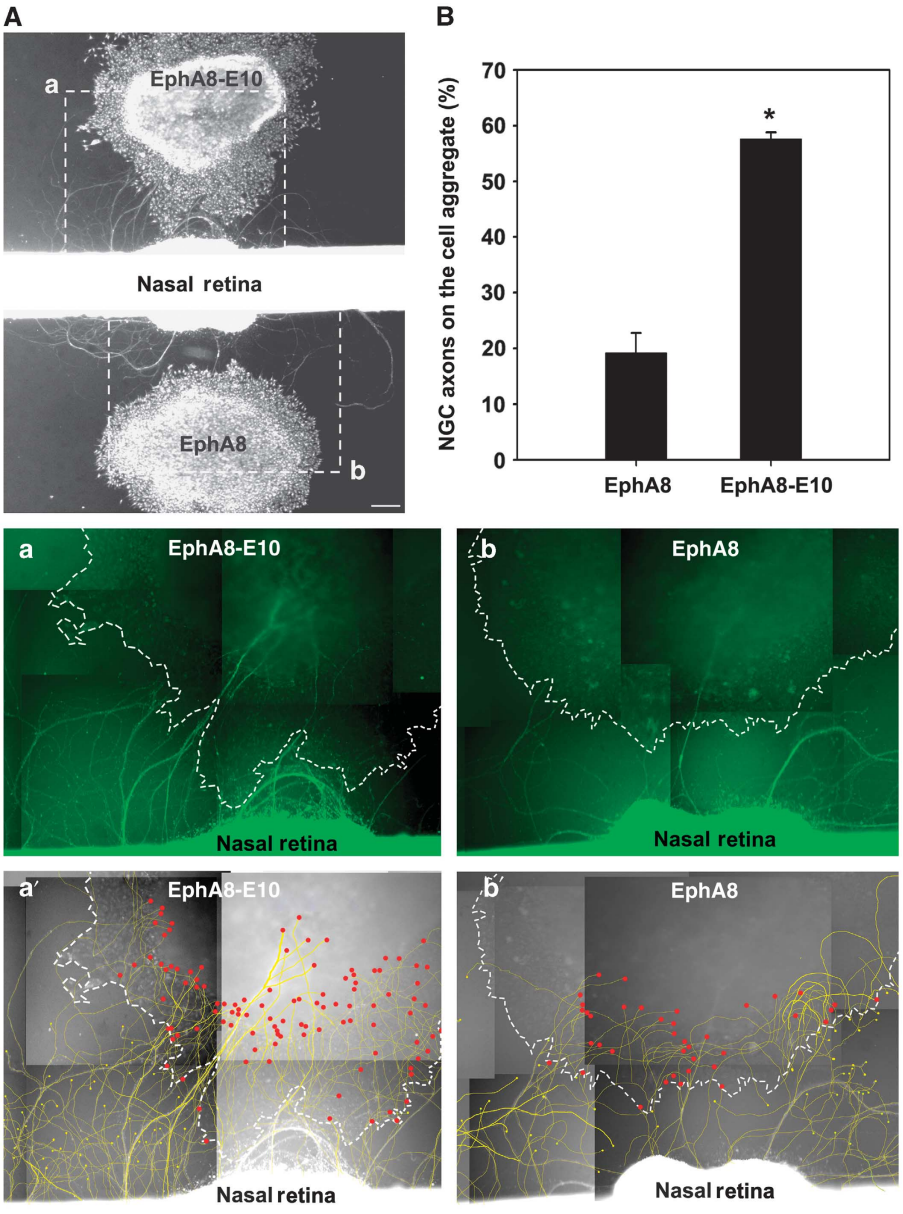

Figure 6 The EphA8-E10 mutant attracts axons from EGFP-labelled nasal RGCs. (**A**) The ventronasal part of the retina was dissected out of the ephrinA5-EGFP Tg embryo (E14.5), and this nasal retinal explant was co-cultured with two distinct HEK293 cell aggregates stably expressing either wild-type EphA8 or the EphA8-E10 mutant. Each cell aggregate was placed on the opposite side of the nasal retinal explant and incubated for 2 days on a coated petri dish. Retinal explants and cell aggregates were stained using a red fluorescent cell tracker to visualize the entire axonal growth pattern out of the retinal explant. (Panels a and b) The dotted boxes (marked by a and b) in **A** are enlarged to show only the EGFP-labelled RGC axons growing on each cell aggregate. The overall boundary of each cell aggregate is outlined by a dotted line. Scale bar = 200 μm. (Panels a′ and b′) These images are identical to that in panels a and b. Many of the EGFP-labelled nasal RGC axons are very thin and could be clearly seen only under higher magnification. Therefore, using Adobe Photoshop, axon images taken under higher magnification were connected to record the detailed image of the entire axonal outgrowth field. Yellow lines mark EGFP-labelled axons growing out of the nasal retina explant, whereas the red circles represent the tip of each axon found within the boundary of each cell aggregate. (**B**) The EGFP-labelled axons on the cell aggregate were compared with the total number of axons growing out of the explant, which were counted by drawing their tracks. Data represent the mean of six different nasal RGC explants ± s.e. (*$P<0.01$, Student's *t*-test).

SC has an important role in regulating the adhesion and repulsion of nasal RGC axons expressing ephrinA. Thus, our data provide the first *in vivo* evidence that Eph receptor–ephrin internalization has a pivotal role in the cellular process converting adhesive signals to repulsive signals on RGC axons, allowing for their proper guidance and mapping.

We show that a particular juxtamembrane region in EphA8 contains the critical domain for endocytosis and that a mutant lacking this domain, EphA8-E10, is an important tool for investigating the functional role of EphA–ephrinA internalization *in vivo*. The peptide motif required for ligand-induced endocytosis lies between residues 587 and 643 in EphA8 and is conserved throughout the other Eph family members (Yoo *et al*, 2010). In addition, we have found that in the absence of this conserved peptide motif, some Eph receptors such as EphA4 and EphB4 are partially defective in ligand-induced endocytosis, suggesting that the endocytotic function of this motif is conserved among Eph receptors

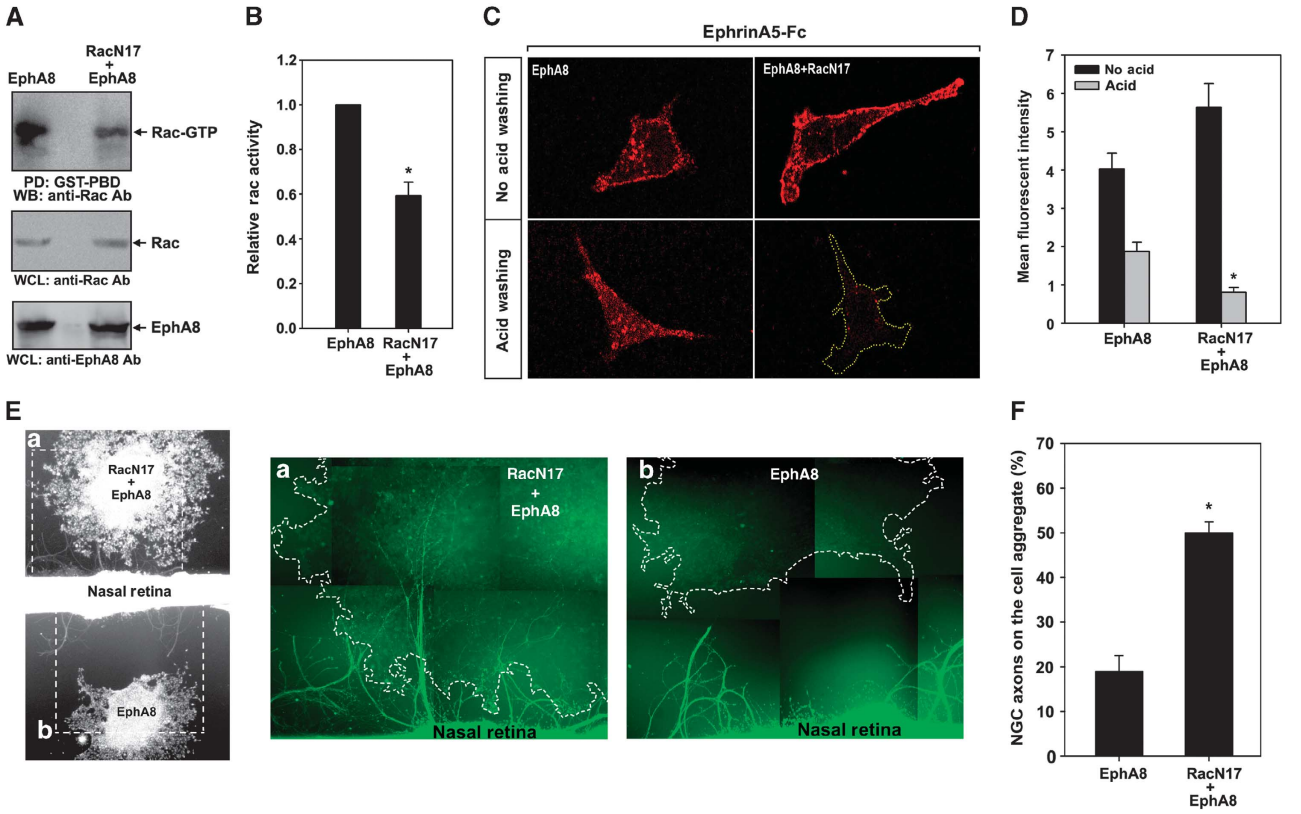

Figure 7 Inhibition of Rac signalling in EphA8-expressing cells impairs trans-endocytosis of ephrinA5 and the repellent behaviour of nasal RGC axons. (**A**) Rac activity was measured by a pull-down assay (PD) of cell extracts prepared from HEK293 cells that stably express the indicated proteins. The GTP-bound form of Rac was precipitated by GST-Pak-1-RBD and probed with anti-Rac1 antibodies (Ab; top panel). Total levels of Rac were visualized by western blotting (WB) with anti-Rac1 Ab (middle panel). The levels of EphA8 were determined by blotting with anti-EphA8 Ab (bottom panel). (**B**) The ratio of GTP-Rac and total Rac levels were quantified and plotted as a bar graph ± s.e. ($n=3$). $^*P<0.001$ versus EphA8 stable cell control (Student's *t*-test). (**C**) Analysis of forward endocytosis in each condition was performed as described in Figure 1A. (**D**) The data in Figure 7C were quantified as described in Figure 1B. Relative binding of ephrinA5-Fc in the EphA8 and RacN17-overexpressing condition was compared with that in the EphA8-expressing condition without or with acid washing ($^*P<0001$; Student's *t*-test). (**E**) *In vitro* retinal explant culture was performed as described in Figure 6A. Two distinct HEK293 cell aggregates that stably express either wild-type EphA8 or both EphA8 and RacN17 were co-cultured with the ventronasal retina from an ephrinA5-EGFP Tg embryo (E14.5). The dotted boxes (marked by a and b) in **E** are enlarged to show only the EGFP-labelled RGC axons growing on each cell aggregate in panels a and b. The dotted line indicates the boundary of each cell aggregate. (**F**) The EGFP-labelled axons on the cell aggregate were compared with the total number of axons growing out of the explant, which were counted by drawing their tracks. Data represent the mean ± s.e. from at least six independent experiments ($^*P<0.01$, Student's *t*-test).

(Yoo *et al*, 2010). This peptide region that is deleted in the EphA8-E10 mutant contains Tyr-615, one of the major autophosphorylation sites. However, phosphorylation at this site was shown to be dispensable for normal tyrosine kinase activity (Choi and Park, 1999). We also observed that the EphA8-E10 mutant retains normal tyrosine kinase activity towards exogenous substrates and that it is autophosphorylated in cultured cells (data not shown). In fact, the tyrosine kinase activity of Eph receptors has been known to be crucial for regulating the endocytotic process (Marston *et al*, 2003; Zimmer *et al*, 2003). In this respect, it is noteworthy that the EphA8-E10 mutant displays such a severe endocytotic defect despite its normal tyrosine kinase activity. Interestingly, our recent study indicated that Rac activity is significantly reduced in cultured cells that express the EphA8-E10 mutant (Yoo *et al*, 2010). Consistent with this finding, Rac activity was remarkably reduced in the anterior SC of the Tg line expressing the EphA8-E10 mutant (Figure 8A). More importantly, inhibition of Rac activity with a RacN17 dominant negative mutant revealed that Rac has an essential role in mediating EphA–ephrinA endocytosis and subsequent retinocollicular map formation *in vivo* (Figure 8C–K). These results strongly support previous reports showing that Rac signalling has a crucial role in the actin polymerization that underlies the internalization of Eph–ephrin complexes (Marston *et al*, 2003; Iwasato *et al*, 2007). A biochemical link between EphA receptors and Rac activity may be provided by upstream regulators of Rac such as guanine nucleotide exchange factors (GEFs), which have been implicated downstream of Eph signalling (Murai and Pasquale, 2005; Egea and Klein, 2007). Our study also indicated that Tiam-1, a Rac1-specific GEF, associates with EphA8 and that this association is greatly reduced in cells expressing the endocytosis-defective EphA8-E10 mutant (Yoo *et al*, 2010). In addition, knockdown of Tiam-1 in these cells disrupts ligand-mediated endocytosis of EphA8, suggesting that Tiam-1 has a role in regulating the endocytosis of EphA receptors (Supplementary Figure S3B–D). However, we observed that Tiam-1 is barely expressed in the SC, suggesting that a different type of Rac-GEF may be involved in mediating EphA-mediated endocytosis in the SC.

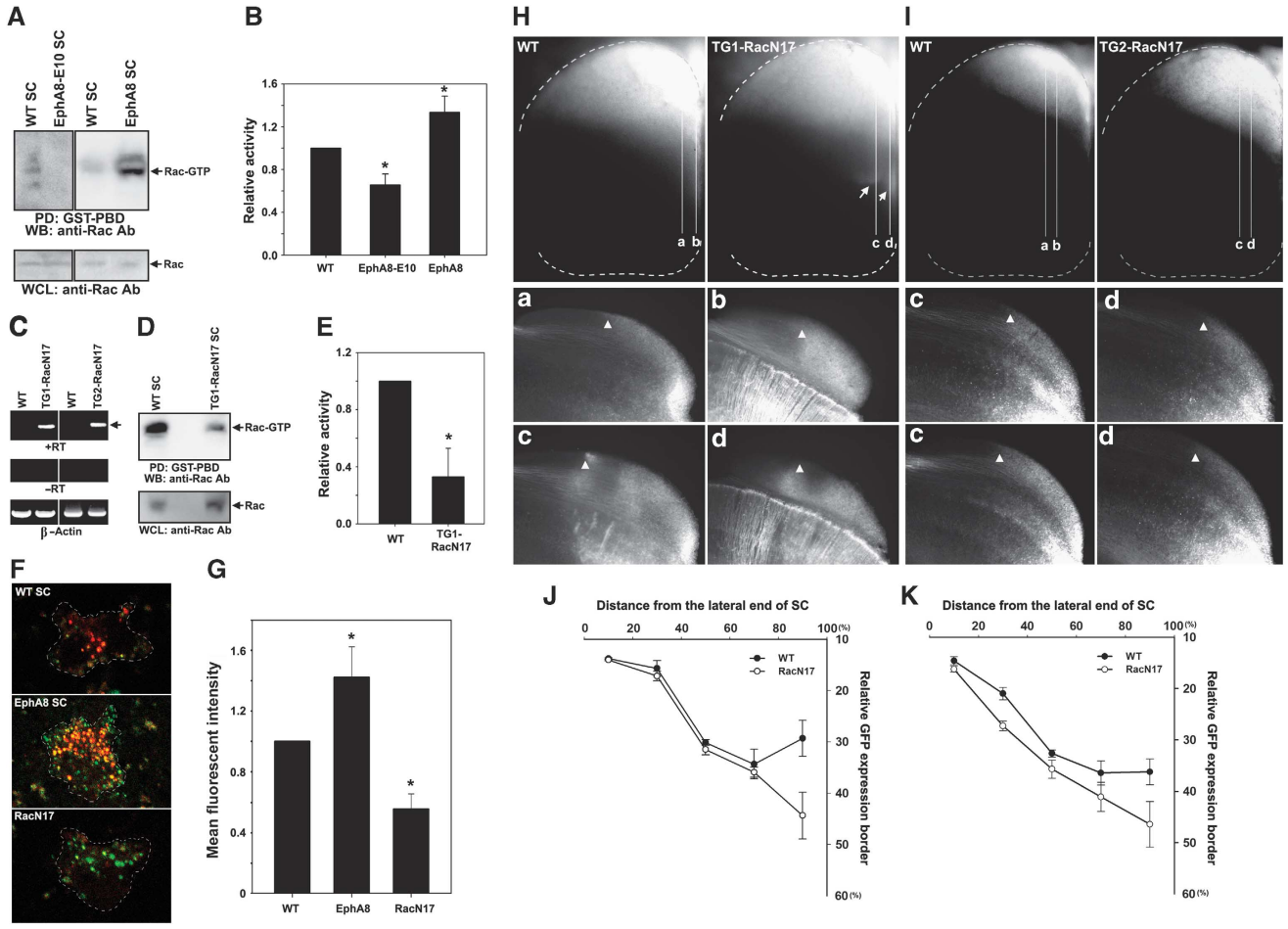

Figure 8 Rac activity is required for EphA endocytosis and retinocollicular map formation. (**A**) The levels of active Rac in extracts from the anterior half of the SC from either EphA8-E10 or EphA8 Tg mice were measured as described in the legend for Figure 7A. Rac activity in different Tg mice was compared with that in wild-type littermates. (**B**) The results of Figure 8A were quantified ($n=3$). *$P<0.01$, ANOVA. (**C**) Expression of RacN17 in two different Tg lines, TG1 and TG2, was analysed by RT–PCR. (**D**) The levels of active Rac in the TG1-RacN17 line. Experiments were performed as described in **A**. (**E**) The data in Figure 8D were quantified ($n=3$). *$P<001$, Student's *t*-test. (**F**) Analysis of forward endocytosis of EphA receptors in primary SC cells from WT, the TG-EphA8 line and the TG1-RacN17 Tg line. Experiments were performed as described in Figure 3F. (**G**) Quantitation of internalized ephrinA5-Fc in Figure 8F represented by mean ± s.e. ($n=40$). *$P<0.01$, ANOVA. (**H**, **I**) The ephrinA5-EGFP line was crossed with two independent RacN17 BAC Tg lines, and their P9 littermates were examined for retinotopic mapping as described in Figure 4. Sagittal sections corresponding to the lines present in the SC are shown in panels a–d. Arrows indicate ectopic termination domains separated from the rest of the nasal retinotopic domain. The arrowhead marks the anterior border of each EGFP-labelled termination domain. (**J**, **K**) Plot illustrating the average position of the anterior border of the EGFP-labelled axon terminations, expressed as a percentage of the anterior–posterior extent of the SC in WT and either TG1 or TG2 line mice, as described in Figure 5C. Statistical data represent the mean of seven SC for TG1 or nine SC for TG2 ± s.e.

Therefore, we propose that the peptide region deleted in the EphA8-E10 mutant constitutes a critical binding site for Rac-GEF, thereby modulating Rac activity, actin polymerization and the subsequent Eph–ephrin internalization (Figure 9).

The next issue is how the EphA8-E10 mutant blocks the normal endocytotic behaviour of other EphA receptors in the anterior SC. In this report, we found that the peptide motif critical for endocytosis is not required for EphA8 to form a complex with EphA4 (Figure 1E). This explains why EphA4 displays severely reduced endocytosis in 293 cells that co-express the EphA8-E10 mutant. These findings further suggest that the EphA8 mutant that lacks the critical domain for endocytosis has a dominant negative role in the endocytosis of EphA receptors in *in vivo* systems such as the retinocollicular topographic mapping system. For example, the EphA8-E10 mutant complexes with other EphA receptors, impairs their interactions with Rac-GEF and reduces Rac activity, thereby blocking their efficient endocytosis, a critical cellular event for converting adhesive cues to repulsive cues for incoming RGC axons (Figure 9). In the anterior SC, some of the EphA family receptors (EphA3, EphA4, EphA5, EphA7 and EphA8) are expressed during a critical time of development of the retinocollicular projection (McLaughlin and O'Leary, 2005; Flanagan, 2006). Their net expression exhibits an A>P gradient in the SC. In *EphA7* knockout mice, the topographic mapping of the nasal RGC axons has been shown to be disrupted, suggesting that the function of EphAs in the anterior SC is to act as a repellent for the nasal RGC axons containing ephrinAs (Rashid *et al*, 2005). We have observed that many aspects of the temporal and spatial expression pattern of EphA8 are very similar to that of EphA7, including the feature that EphA8 is not expressed in RGCs during the development of the retinocollicular projection (unpublished result). Nevertheless, we have observed that, in EphA8 null

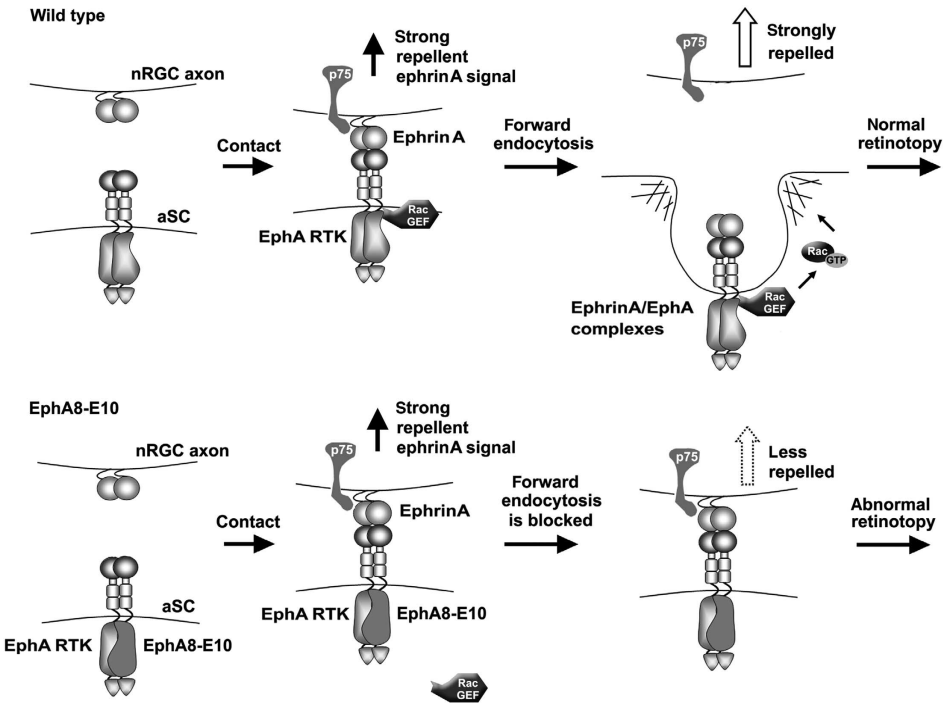

Figure 9 Model in which ephrinA trans-endocytosis into EphA-expressing SC cells regulates the repellent activity of nasal RGC axons. Contact of EphA-expressing cells with ephrinA-expressing axons induces the ephrinA–p75^{NTR} complex to mediate a reverse signalling for axon repulsion but also induces the EphA–RacGEF complex to modulate Rac activity and actin polymerization, the possible critical events for Eph–ephrin endocytosis. EphA–ephrinA endocytotic processes cause destabilization of cell–cell contacts and initiate cell–cell detachment. Without involvement of these endocytotic processes, the ephrinA reverse signalling would not effectively lead to retraction of the nasal RGC axons away from anterior SC cells despite its potential repellent activity. One possible function of the exon10-encoded peptide region in EphA8 is to form a binding site for Rac-GEF critical for Eph–ephrin endocytosis. The EphA8-E10 mutant lacking this peptide region is defective in activating Rac signalling when it is bound to ephrinAs. Importantly, the EphA8-E10 mutant protein associates with other EphA receptors in the anterior SC. Therefore, after cell–cell contact, ephrinA–EphA complexes are not efficiently internalized into EphA8-E10-expressing cells. These enhanced adhesive events seem to override the repellent ephrinA reverse signal triggered by ephrinA–p75^{NTR} complex, resulting in abnormal development of the retinocollicular topography.

mutant mice, essentially all RGC axons normally terminate at their topographically appropriate positions in the SC (data not shown). These results are not surprising because only one of several EphAs with A>P gradient expression is eliminated from the SC. In this respect, the dominant negative approach is more appropriate for studying the functional roles of EphA receptors in retinocollicular topographic mapping. Consistent with this prediction, we show that, in Tg mice expressing the endocytosis-defective EphA8 receptor, the primary SC cells with EphA receptors display a significant reduction in Rac activity and the subsequent endocytotic behaviour. These findings suggest that the endocytosis-defective EphA8 protein is a powerful tool for overcoming the compensatory effects of EphA family members *in vivo*.

BAC Tg technology provides an ideal *in vivo* expression system for recapitulating the temporal and spatial regulation of the *EphA8* gene, as its large genomic size (~150 kbp) would be expected to contain all necessary *cis*-acting regulatory elements and locus control regions. In addition, introducing modifications to BAC DNA, such as the small deletion of exon 10 in EphA8, is expedited by well-established methods using a bacterial homologous recombination system (Yu *et al*, 2000; Zhang *et al*, 2000; Heintz, 2001; Gong *et al*, 2003). We have found that BAC Tg mice expressing wild-type EphA8 or endocytosis-defective mutant have no obvious defects in the SC, including defects related to the size of the SC and the expression patterns of ephrinAs or EphAs (Supplementary Figure S2). In addition, our quantitative RT–PCR analysis shows that the levels of ectopic EphA8-E10 transcripts are not higher than that of endogenous EphA8 (Supplementary Figure S1D), suggesting that BAC Tg technology is most useful for inducing endogenous gene expression. In contrast, we have found that EphA8-E10 protein levels are consistently higher than that of endogenous EphA8, that is, EphA8-E10 protein levels were three-fold greater in SC extract (Supplementary Figure S1E) and at least two-fold greater in 293 cells (Figure 1E). This increase in EphA8-E10 protein would be expected if the EphA8 mutant undergoes slower protein degradation due to its defective endocytotic behaviour. On the other hand, this increased protein stability of EphA8-E10 is likely more favourable for its dominant negative role against EphA receptors that show an overlapping expression pattern in the anterior SC. In support of this dominant negative role, anterograde labelling techniques show that nasal RGC axons exhibit mapping defects, with these axons forming ectopic TZs in the anterior SC and the correct TZ in the posterior SC. The aberrant mapping that we have observed in the two different EphA8-E10 BAC Tg lines is reproducibly consistent, and the penetrance of the mapping defects is about 70–80% depending on each Tg line. This finding is similar to what has been reported for topographic mapping defects in *EphA7* knockout mice (Rashid *et al*, 2005). Intriguingly, in our Tg lines and in *EphA7* knockout

mice, the ectopic TZs are found in the anterior SC and not closer to the correct TZ in the posterior SC. These results suggest that most nasal RGC axons target their correct topographic site in the posterior SC and that only a small proportion miss the target, with a large anterior shift. One possible interpretation regarding this phenotype is that only a small subset of anterior SC cells has severe defects in trans-endocytosis of ephrinAs, thereby affecting a small proportion of the nasal RGC axons that respond best to these SC cells. The magnitude of the diminished repellent activity of the severely affected SC cells would be mostly dependent on the overlapping expression of EphA8-E10 with other EphA receptors. It also seems that the anterior shift in retinotopic mapping in the SC was manifested much more medially than laterally (see Figures 4 and 8). This result was expected because EphA receptors were more strongly expressed in a region close to the midline of the SC (Supplementary Figures S1 and S2). In the medial region, the magnitude of the diminished repellent activity was greater as those SC cells are more strongly affected by high levels of EphA8-E10. In two different compound Tg lines, essentially all littermates expressing the endocytosis-defective EphA8 mutant showed anteriorly expanded TZs in the SC. Although the aberrant mapping pattern is very consistent, the magnitude of the phenotype appeared to vary between two different Tg lines, possibly because of different expression levels of the endocytosis-defective EphA8 protein, which depends on the BAC copy number inserted into the genome of each mouse line. In conclusion, the similarity of the mapping defects in the two distinct EphA8-E10 Tg mice strongly supports our hypothesis that the EphA8 mutant forms complexes with other EphA receptors in the anterior SC and that it effectively inhibits their trans-endocytosis of ephrinAs, thereby diminishing the repellent effects of these receptors on the incoming nasal axons. Nevertheless, we do not rule out an alternative possibility that the effects of the EphA8-E10 mutant on nasal axons are simply adhesive and that they do not have dominant negative effects *in vivo*.

On the other hand, it is possible that the extracellular domain of EphA8-E10 *per se* contributes to the topographic mapping in the ephrinA^{nasalRGC}/EphA^{anteriorSC} module. This possibility has been raised by previous reports that reverse signalling initiated by ephrinAs upon binding EphAs controls axon guidance and mapping (Rashid *et al*, 2005; Lim *et al*, 2008). For example, ephrinA-expressing retinal axons are repelled from stripes containing EphA7-Fc when given the choice between EphA7-Fc and control Fc *in vitro*. In these reports, it was impossible to address whether the intracytoplasmic region of EphAs and their forward endocytosis have an important role in mediating the repellent effect on ephrinA reverse signalling. However, if the EphA extracellular domain is responsible for inducing the repellent activity on ephrinAs without involving its intracytoplasmic region, we would expect that the appropriate nasal RGC axons would show higher levels of repellent activity and that their termination domains would become posteriorly shifted toward the end of the SC. This prediction was true for the EphA8-overexpressing mice, but not EphA8-E10 mutant mice (Figure 5), suggesting that the EphA-intracytoplasmic region also contributes to the topographic mapping in the ephrinA^{nasalRGC}/EphA^{anteriorSC} module. An argument against our hypothesis is that the EphA8-E10 mutant may not be an appropriate tool for addressing the relevance of Eph–ephrin endocytosis *in vivo*, possibly because of its altered kinase activity or signalling properties. However, our experiments with mice that express RacN17 under the control of the EphA8 promoter revealed that inhibition of Rac activity disrupts not only normal endocytosis of EphA in the anterior SC but also the subsequent nasal RGC axonal repulsion. This aberrant phenotype is identical to what we observed in mice that express the EphA8-E10 mutant. These findings are especially important because inhibition of Rac activity is likely to disrupt the endocytotic mechanism without grossly affecting signalling or proteolytic cleavage of redundant Eph receptors. In conclusion, our finding that wild-type EphA8 and the EphA8-E10 mutant are associated with opposite mapping defects strongly indicates that, at least in the ephrinA^{nasalRGC}/EphA^{anteriorSC} module, endocytosis of EphAs has a critical role in converting adhesive signals to repellent signals on incoming nasal RGC axons.

An important issue is how ephrinA that is trans-endocytosed into EphA-expressing SC cells regulates the repellent activity of nasal RGC axons. A recent study revealed that p75^{NTR} is a signalling partner for ephrinAs. For example, p75^{NTR} null mice have aberrant anterior shifts in retinal axon terminations in the SC, and this phenotype can be explained by a reduced repellent activity of ephrinAs present on the nasal RGC axons (Lim *et al*, 2008). By integrating these results with our current findings, we propose that contact of EphA-expressing SC cells with ephrinA-expressing nasal RGC axons induces two distinct protein complexes on the apposing cells: the ephrinA–p75^{NTR} complex on the nasal axon and EphA–RacGEF complex on the anterior SC cell (Figure 9). The ephrinA–p75^{NTR} complex triggers a reverse signalling pathway inducing repellent activity of ephrinAs on the nasal RGC axons. Simultaneously, EphA–RacGEF complex also induces trans-endocytosis of ephrinAs into EphA cells and begins to destabilize cell–cell contact. The balance between adhesion and repulsion becomes favoured towards repulsion when a forward endocytosis normally allows cell–cell detachment to take place. If endocytosis were defective, the adhesive signal would predominate over the repellent signal by the ephrinA–p75^{NTR} complex, and the outcome would be abnormal development of the retinocollicular topography as we observed in the EphA8-E10 mutant mice (Figure 9).

Materials and methods

Cell culture and expression plasmids

HEK293 cells were cultured as described previously (Gu *et al*, 2005). EphA4, EphA8 or RacN17 cDNA subcloned into the pcDNA3neo expression vector was stably transfected into HEK293 cells as described previously (Choi and Park, 1999). Transient transfection was performed using Metafectin (Biontax) according to the manufacturer's instructions. For SC neuron and RGC culture, the anterior half of the dorsal midbrain and nasal retina were isolated from the E14.5 mouse embryo, respectively, as described previously (Shin *et al*, 2007; Lim *et al*, 2008).

To construct EphA8-E10 (with a deletion of amino acids (aa) 588–643 of mouse EphA8), we amplified a 281 bp PCR product using primers matching nucleotides (nt) 1570–1590 (5′-GTGTCAGG CCTCAAACCAGG-3′) and nt 1823–1840 (5′-CCTGACTCCCCCTGT CCGTTCTGGTAAT-3′) of the EphA8 cDNA, as well as a 260 bp PCR product using primers matching nt 2006–2024 (5′-ACGGACAGGGG GAGTCAGGAGAAGTGTG-3′) and nt 2236–2255 (5′-GTCCTGAGGAA GGCATCTAG-3′) of the EphA8 cDNA. The underlined nucleotides

represent the sequence matching the specific nt number. The resulting two partially complementary PCR fragments were annealed and used as a template in another PCR performed with primers matching nt 1570–1590 and nt 2236–2255 of the EphA8 cDNA. Next, the 521 bp PCR product was digested with *Nsi*I/*Xba*I and subcloned into the corresponding region of full-length EphA8 cDNA. The same procedures were used to generate the EphA8-E9 construct, except that different primers were used. A 531 bp PCR product was amplified using primers matching nt 1232–1250 (5′-TCCCGCAGCAGACAAGCCT-3′) and nt 1755–1772 (5′-GGTG GGGGTGCTCTTCTTGCAGATGAGA-3′) of EphA8 cDNA, and a 164 bp PCR product was amplified using primers matching nt 1841–1858 (5′-GCAAGAAGAGCACCCCCACCTGTCTTCT-3′) and nt 1977–1994 (5′-ATCTTCTCAATGTGGATC-3′) of EphA8 cDNA. Mouse EphA8 tagged with the nine amino-acid hemagglutinin (HA) epitope (YPYDVPDYA) at its COOH terminus has been described elsewhere (Gu and Park, 2001), and EphA8-E10 or EphA8-E9 tagged with a HA epitope was generated by subcloning its internal fragment into the corresponding region of the wt EphA8-HA DNA. To generate the ephrinA5-IRES-EGFP construct, we subcloned the 1.1 kbp ephrinA5 cDNA insert into the XhoI site of the pIRES2-EGFP vector (Invitrogen). Human dominant negative mutant Rac1(RacN17) cDNA tagged with a HA epitope at its NH2 terminus in pcDNA3 expression vector has been described elsewhere (Zhang *et al*, 1995). The mouse Tiam-1 expression plasmid was generously gifted by Dr van der Kammen RA (Division of Cell Biology, The Netherlands Cancer Institute, Amsterdam, The Netherlands).

Endocytosis, immunofluorescence staining, immunoprecipitation, western blot, Rac activity assay and RNA interference

For the endocytosis assay, cells were plated at a density of 1×10^6 cells per 35 mm dish and transiently transfected as described above. At 24 h post-transfection, cells (2×10^5) were seeded onto coverslips coated with fibronectin (20 μg/ml, Sigma). After an additional 24 h, cells were incubated with medium containing 0.5% serum for 3 h. EphrinA5-Fc or EphA8-Fc (2 μg/ml) was pre-clustered with goat anti-human Fc (Jackson ImmunoResearch Laboratories Inc.) and then incubated with culture medium for 30 min at 37°C. To remove the cell-surface-bound Fc-fusion proteins, we treated the cells three times with acid buffer (0.2 M acetic acid and 0.5 M NaCl) for 10 min on ice. Cells were gently washed twice with phosphate-buffered saline (PBS), fixed with 4% paraformaldehyde–2% sucrose in PBS on ice for 10 min, rinsed with PBS and blocked for 30 min at room temperature with 3% bovine serum albumin, 5% horse serum and 0.1% Triton X-100 in PBS. For immunofluorescence staining of Fc-fusion proteins, Texas Red dye-conjugated goat anti-human IgG was applied for 60 min as described previously (Shin *et al*, 2007). For endocytosis assays in primary cultured cells, dissociated cells (2×10^4) were seeded onto a cover glass coated with poly-L-lysine (10 μg/ml, Sigma) and laminin (10 μg/ml, Sigma), and they were then cultured in Neurobasal medium (Invitrogen) containing either N-2 supplement (Invitrogen) for SC cells or B-27 (Invitrogen) for RGCs. After 24 h, the medium was carefully replaced with fresh, pre-warmed medium and cells were further incubated for 24 h. After treatment with pre-clustered ephrinA5-Fc or EphA8-Fc, cells were washed twice with acid buffer for 1 min to remove cell-surface-bound Fc-fusion proteins. Cells were then permeabilized and processed for immunofluorescence staining as described above. Staining for surface and total Fc fusion proteins in the SC cells was performed and calculated, respectively, as described elsewhere (Zimmer *et al*, 2003). Briefly, SC cells were incubated with FITC-conjugated anti-goat human IgG for 60 min, washed with PBS and then permeabilized for 5 min with ice cold 0.1% Triton X-100 in PBS at room temperature. Cells were then incubated with Texas Red dye-conjugated anti-goat human IgG for total staining. Cells were mounted with Vectashield (Vector Laboratory) and imaged using a confocal microscope (model FV300; Olympus). For each experiment, 30–50 cells were analysed using NIH ImageJ software. Fluorescent intensity of each cell was measured and adjusted for local background before obtaining a mean fluorescent intensity per cell for each assay group. Immunoprecipitation and western blot analysis were performed essentially as described previously (Gu and Park, 2001). Rac activity assay and Tiam1-specific RNA interference were performed as described previously (Yoo *et al*, 2010).

Targeting vector for BAC modification and BAC Tg mice

EphA8 BAC Tg mice expressing LacZ have already been described (Kim *et al*, 2007). To generate the EphA8-E10 mutant, we synthesized the homology arms A and B that flank mouse EphA8 exon 10 by performing PCR using the following primer sets: 5′-CTCGAGCCAGAACGGGCAGGGTGA-3′ (forward primer for A arm), 5′-CTCGAGAAGGAGAAGGGCCCTCAA-3′ (reverse primer for A arm), 5′-GCGGCCGCGAGGCCGGGAGGGAT-3′ (forward primer for B arm) and 5′-GCGGCCGCAGACTGGACTCCCGT-3′ (reverse primer for B arm). The underlined nucleotides mark the core sequence matching the template DNA, excluding the restriction enzyme site. The targeting vector was constructed using the pGEM11Z vector (Promega) as follows. First, pGEM11Z was digested with *Xba*I and then a frt-Kana-frt cassette was inserted into this site. Second, the homology arm A was cloned into the XhoI site right before the first frt sequence in pGEM11Z and then a B arm was inserted into the NotI site present right after the second frt sequence. This targeting vector was digested with *Sfi*I/*Nsi*I and then inserted specifically into the EphA8 BAC genomic DNA (RP23-357K18) using a bacterial homologous recombination method as described previously (Kim *et al*, 2007). For ephrinA5-EGFP BAC, homology arms A and B flanking the mouse ephrinA5 transcription start site (ATG) were synthesized by PCR using the following primer sets: 5′-GGCCAAGTCGGCCGGTGTATGTCTCCCCGCAGCCGC-3′ (forward primer for A arm), 5′-GAGCTCGGAGATCGGGGATCCAG-3′ (reverse primer for A arm), 5′-GCGGCCGCTGCTCTTTCTGGTGCTCT GG-3′ (forward primer for B arm) and 5′-ATGCATCTTTCCACT CACCCATCCCT-3′ (reverse primer for B arm). The homology A arm was subcloned into the Sfil/SacI site before the frt-Kana-frt cassette in pGEM11Z. Next, a loxP-flanked EGFP reporter was subcloned between the A arm and kanamycin cassette. The homology B arm was then inserted into the NotI/NsiI site after the kanamycin cassette. This targeting vector was digested with *Sfi*I/*Nsi*I and inserted by bacterial homologous recombination into the ephrinA5 BAC genomic DNA (RP23-23O22) as described above. To generate the RacN17 mutant, the 620 bp HA-RacN17 cDNA was inserted in place of LacZ into the previous targeting vector for EphA8-LacZ mice. This modified targeting vector was digested with *Sfi*I and inserted by bacterial homologous recombination into the EphA8 BAC genomic DNA (RP23-357K18) as described above. ICR was used to produce Tg mice as described previously. BAC Tg mice were identified by PCR analysis of DNA extracted from tail biopsy specimens. For EphA8-LacZ, a 250 bp sequence was amplified with primers 5′-GCGGGAGAGGCAGGAGCGCGCCA-3′ and 5′-CGGAAACC AGGCAAAGCGCCAT-3′. For EphA8-E10, a 250 bp sequence was amplified with primers 5′-GGCGTGTGTGAACTCCTTTTCTTA-3′ and 5′-TGAAGTAGGTCTCTGCAGTGTCG-3′. For ephrinA5-EGFP, a 450 bp sequence was amplified with primers 5′-CTGGATCCCCGATCTCTCC-3′ and 5′-CCGTCGTCCTTGAAGAAGATGGTGC-3′. For HA-RacN17, a 260 bp sequence was amplified with primers 5′-CCTTATGATGTGC-CAGATTAT-3′ and 5′-GTTTGCGGATAGGATAGGGG-3′.

In situ RNA hybridization

Paraffin sagittal sections (10 μm thick) obtained from P4 mice brains were hybridized with the relevant RNA probes according to the previous procedure (Shim *et al*, 2007). Single-stranded RNA probes labelled with digoxigenin-UTP were synthesized from linearized template DNA as directed by the manufacturer (Roche). Fragments matching nt 1714–1930, 1974–2236 and 2992–3206 of the mouse EphA8 cDNA sequence (GenBank accession no. NM_007939); nt 256–573, 616–823 and 848–1052 of the mouse ephrinA5 cDNA sequence (GenBank accession no. NM_207654); nt 1555–1849, 1869–2073 and 2891–3118 of the mouse EphA4 cDNA sequence (GenBank accession no. NM_007936); and nt 1513–1756, 1760–1953 and 2801–2988 of the EphA7 cDNA sequence (GenBank accession no. BC026153) were used as templates for riboprobe synthesis. X-gal staining of whole-mounted midbrains from P5 EphA8-LacZ Tg mice was carried out as described previously (Park *et al*, 1997).

Axon tracing analysis

Anterograde labelling was performed according to the protocol using DiI (Molecular Probes; Lim *et al*, 2008). Briefly, P9 EphA8-E10 Tg mice and their wild-type littermates were injected with DiI into the ventronasal retina using a Picospritzer II (General Valve). About 36 h later, the mice were anesthetized and transcardially perfused with 4% paraformaldehyde. The TZ in the whole-mounted

midbrain as well as the injection site in the flat-mounted retina was visualized by fluorescence imaging. Every midbrain was sectioned on a vibratome (Vibratome 1000) into 100-μm-thick slices for the analysis of the branch and arborization of axons at higher magnification.

EGFP-labelled axon terminals in the SC were digitally analysed using Adobe Photoshop and Adobe Illustrator, and statistically analysed with Excel and Sigma Plot. Photographs of whole-mount brains were captured using the same fluorescence intensity with Hamamatsu Photonics (ORCA-ER) and collected on the same photo layer in Adobe Photoshop. The grey scale in this layer was synchronously normalized until pixels representing the EGFP-positive zone were black and those representing the EGFP-negative zone were white, resulting in a grey scale value range of 0–255. The SC was divided into five or 10 equal segments along the LM axis, and the distance between the posterior ends of the SC and the anterior border of the black pixels was measured and divided by the total length of SC in each segment.

Retinal explant culture

For co-culture with primary retinal axons, HEK293 cells stably expressing EphA8, EphA8-E10 or RacN17 were grown to 90% confluence, washed three times with PBS and dissociated into small cell aggregates by gentle pipetting. Similar-sized cell aggregates from each cell line were seeded on a 60 mm bacterial petri dish coated with 10 μg/ml poly-L-lysine and 10 μg/ml laminin. The ventronasal or dorsotemporal retina was dissected from E14.5 embryos (ephrinA5-EGFP BAC Tg) and attached to a sterile cellulose nitrate filter (Whatman). The filter containing the retinal tissue was then placed on the midline between the two different cell aggregates (separated by 0.4 mm from each other). A few hours after co-culture onset, we re-examined whether each cell clump looked similar in size and was equally distant from the explant. These were important criteria for our co-culture experiments. If the status of each cell clump did not meet our standards, 2 days of co-culture were not continued. When the nasal RGC explant and cell clumps satisfied our criteria, they were allowed to grow for 2 additional days. We always found that the cell clump with EphA8-E10 became much closer to the explant, possibly because of adhesive interactions between the cell clump and the ingrowing axons. During 2 days of culture, most axons growing out of the explant were long enough to extend past the cell clump. Some of the axons remained short, and most of them did not contain a large growth cone under higher magnification, suggesting that those axonal tips had retracted or collapsed upon encountering a repulsive cue such as EphA receptors. After 2 days, the red-fluorescent cell tracker dye, CMPTX (Molecular Probes), was added to the culture medium to stain all living cells. The red and EGFP fluorescent images were photographed independently using Hamamatsu Photonics (ORCA-ER). The outline of aggregates and the ventronasal axons labelled with EGFP were plotted in the red and green fluorescent images, respectively. With all axons marked, the ratio of axons located on each aggregate was calculated.

Antibodies

Polyclonal anti-EphA8 antibody specific for the EphA8 juxtamembrane region has been described previously (Choi and Park, 1999). Polyclonal rabbit anti-HA antibodies were obtained from Zymed. Polyclonal rabbit anti-EphA4 antibody and anti-Tiam1 were purchased from Santa Cruz Biotechnology. Polyclonal rabbit anti-actin antibody was purchased from Sigma-Aldrich Chemical Co. Monoclonal mouse anti-Rac1 was purchased from BD Biosciences. Goat anti-human IgG was acquired from Jackson ImmunoResearch Laboratories Inc. Texas Red dye-conjugated goat anti-human IgG and FITC-conjugated goat anti-human IgG were from Chemicon.

Supplementary data

Supplementary data are available at *The EMBO Journal* Online (http://www.embojournal.org).

Acknowledgements

We are indebted to Jongae Shin and Changkyu Gu for various EphA8 mutants. We also thank Yoo-Shick Lim and Dennis O'Leary for technical assistances and helpful discussions. This work was supported by a grant (no. 2009-0083149) from Korea Science and Engineering Foundation (KOSEF) and a grant (no. 2009K001246) from Brain Research Center of the 21st Century Frontier Research Program funded by the Ministry of Education, Science and Technology, the republic of Korea.

Author contributions: Sooyeon Yoo, Yujin Kim, Hyuna Noh, Haeryung Lee and Eunjeong Park participated in the study and the specific contribution was as follows: acquisition, analysis, interpretation and statistical analysis of the data. Soochul Park participated in the study and the specific contribution was as follows: conception and design of the research, obtaining funding, drafting of the manuscript and supervision.

Conflict of interest

The authors declare that they have no conflict of interest.

References

Batlle E, Bacani J, Begthel H, Jonkheer S, Gregorieff A, van de Born M, Malats N, Sancho E, Boon E, Pawson T, Gallinger S, Pals S, Clevers H (2005) EphB receptor activity suppresses colorectal cancer progression. *Nature* **435:** 1126–1130

Bruckner K, Klein R (1998) Signaling by Eph receptors and their ephrin ligands. *Curr Opin Neurobiol* **8:** 375–382

Choi S, Park S (1999) Phosphorylation at Tyr-838 in the kinase domain of EphA8 modulates Fyn binding to the Tyr-615 site by enhancing tyrosine kinase activity. *Oncogene* **18:** 5413–5422

Cowan CA, Henkemeyer M (2001) The SH2/SH3 adaptor Grb4 transduces B-ephrin reverse signals. *Nature* **413:** 174–179

Egea J, Klein R (2007) Bidirectional Eph-ephrin signaling during axon guidance. *Trends Cell Biol* **17:** 230–238

Feldheim DA, Nakamoto M, Osterfield M, Gale NW, DeChiara TM, Rohatgi R, Yancopoulos GD, Flanagan JG (2004) Loss-of-function analysis of EphA receptors in retinotectal mapping. *J Neurosci* **24:** 2542–2550

Flanagan JG (2006) Neural map specification by gradients. *Curr Opin Neurobiol* **16:** 59–66

Flanagan JG, Vanderhaeghen P (1998) The ephrins and Eph receptors in neural development. *Annu Rev Neurosci* **21:** 309–345

Frisen J, Yates PA, McLaughlin T, Friedman GC, O'Leary DD, Barbacid M (1998) Ephrin-A5 (AL-1/RAGS) is essential for proper retinal axon guidance and topographic mapping in the mammalian visual system. *Neuron* **20:** 235–243

Gong S, Zheng C, Doughty ML, Losos K, Didkovsky N, Schambra UB, Nowak NJ, Joyner A, Leblanc G, Hatten ME, Heintz N (2003) A gene expression atlas of the central nervous system based on bacterial artificial chromosomes. *Nature* **425:** 917–925

Gu C, Park S (2001) The EphA8 receptor regulates integrin activity through p110gamma phosphatidylinositol-3 kinase in a tyrosine kinase activity-independent manner. *Mol Cell Biol* **21:** 4579–4597

Gu C, Shim S, Shin J, Kim J, Park J, Han K, Park S (2005) The EphA8 receptor induces sustained MAP kinase activation to promote neurite outgrowth in neuronal cells. *Oncogene* **24:** 4243–4256

Hattori M, Osterfield M, Flanagan JG (2000) Regulated cleavage of a contact-mediated axon repellent. *Science* **289:** 1360–1365

Heintz N (2001) BAC to the future: the use of bac transgenic mice for neuroscience research. *Nat Rev Neurosci* **2:** 861–870

Holland SJ, Gale NW, Mbamalu G, Yancopoulos GD, Henkemeyer M, Pawson T (1996) Bidirectional signalling through the EPH-family receptor Nuk and its transmembrane ligands. *Nature* **383:** 722–725

Iwasato T, Katoh H, Nishimaru H, Ishikawa Y, Inoue H, Saito YM, Ando R, Iwama M, Takahashi R, Negishi M, Itohara S (2007) Rac-GAP alpha-chimerin regulates motor-circuit formation as a key mediator of EphrinB3/EphA4 forward signaling. *Cell* **130:** 742–753

Janes PW, Saha N, Barton WA, Kolev MV, Wimmer-Kleikamp SH, Nievergall E, Blobel CP, Himanen JP, Lackmann M, Nikolov DB (2005) Adam meets Eph: an ADAM substrate recognition module acts as a molecular switch for ephrin cleavage in trans. *Cell* **123:** 291–304

Kim Y, Song E, Choi S, Park S (2007) Engineering lacZ reporter gene into an ephA8 bacterial artificial chromosome using a highly efficient bacterial recombination system. *J Biochem Mol Biol* **40:** 656–661

Klein R (2009) Bidirectional modulation of synaptic functions by Eph/ephrin signaling. *Nat Neurosci* **12:** 15–20

Knoll B, Drescher U (2002) Ephrin-As as receptors in topographic projections. *Trends Neurosci* **25:** 145–149

Konstantinova I, Nikolova G, Ohara-Imaizumi M, Meda P, Kucera T, Zarbalis K, Wurst W, Nagamatsu S, Lammert E (2007) EphA-Ephrin-A-mediated beta cell communication regulates insulin secretion from pancreatic islets. *Cell* **129:** 359–370

Kullander K, Klein R (2002) Mechanisms and functions of Eph and ephrin signalling. *Nat Rev Mol Cell Biol* **3:** 475–486

Lim YS, McLaughlin T, Sung TC, Santiago A, Lee KF, O'Leary DD (2008) p75(NTR) mediates ephrin-A reverse signaling required for axon repulsion and mapping. *Neuron* **59:** 746–758

Marler KJ, Becker-Barroso E, Martinez A, Llovera M, Wentzel C, Poopalasundaram S, Hindges R, Soriano E, Comella J, Drescher U (2008) A TrkB/EphrinA interaction controls retinal axon branching and synaptogenesis. *J Neurosci* **28:** 12700–12712

Marston DJ, Dickinson S, Nobes CD (2003) Rac-dependent trans-endocytosis of ephrinBs regulates Eph-ephrin contact repulsion. *Nat Cell Biol* **5:** 879–888

McLaughlin T, O'Leary DD (2005) Molecular gradients and development of retinotopic maps. *Annu Rev Neurosci* **28:** 327–355

Murai KK, Pasquale EB (2005) New exchanges in eph-dependent growth cone dynamics. *Neuron* **46:** 161–163

Park S, Frisen J, Barbacid M (1997) Aberrant axonal projections in mice lacking EphA8 (Eek) tyrosine protein kinase receptors. *EMBO J* **16:** 3106–3114

Pasquale EB (2005) Eph receptor signalling casts a wide net on cell behaviour. *Nat Rev Mol Cell Biol* **6:** 462–475

Pasquale EB (2008) Eph-ephrin bidirectional signaling in physiology and disease. *Cell* **133:** 38–52

Rashid T, Upton AL, Blentic A, Ciossek T, Knoll B, Thompson ID, Drescher U (2005) Opposing gradients of ephrin-As and EphA7 in the superior colliculus are essential for topographic mapping in the mammalian visual system. *Neuron* **47:** 57–69

Reber M, Burrola P, Lemke G (2004) A relative signalling model for the formation of a topographic neural map. *Nature* **431:** 847–853

Segura I, Essmann CL, Weinges S, Acker-Palmer A (2007) Grb4 and GIT1 transduce ephrinB reverse signals modulating spine morphogenesis and synapse formation. *Nat Neurosci* **10:** 301–310

Shim S, Kim Y, Shin J, Kim J, Park S (2007) Regulation of *EphA8* gene expression by TALE homeobox transcription factors during development of the mesencephalon. *Mol Cell Biol* **27:** 1614–1630

Shin J, Gu C, Park E, Park S (2007) Identification of phosphotyrosine binding domain-containing proteins as novel downstream targets of the EphA8 signaling function. *Mol Cell Biol* **27:** 8113–8126

Wilkinson DG (2000) Topographic mapping: organising by repulsion and competition? *Curr Biol* **10:** R447–R451

Wilkinson DG (2001) Multiple roles of EPH receptors and ephrins in neural development. *Nat Rev Neurosci* **2:** 155–164

Xu NJ, Henkemeyer M (2009) Ephrin-B3 reverse signaling through Grb4 and cytoskeletal regulators mediates axon pruning. *Nat Neurosci* **12:** 268–276

Yamaguchi Y, Pasquale EB (2004) Eph receptors in the adult brain. *Curr Opin Neurobiol* **14:** 288–296

Yoo S, Shin J, Park S (2010) EphA8-ephrinA5 signaling and clathrin-mediated endocytosis is regulated by Tiam-1, a Rac-specific guanine nucleotide exchange factor. *Mol Cells* **29:** 603–609

Yu D, Ellis HM, Lee EC, Jenkins NA, Copeland NG, Court DL (2000) An efficient recombination system for chromosome engineering in *Escherichia coli*. *Proc Natl Acad Sci USA* **97:** 5978–5983

Zhang S, Han J, Sells MA, Chernoff J, Knaus UG, Ulevitch RJ, Bokoch GM (1995) Rho family GTPases regulate p38 mitogen-activated protein kinase through the downstream mediator Pak1. *J Biol Chem* **270:** 23934–23936

Zhang Y, Muyrers JP, Testa G, Stewart AF (2000) DNA cloning by homologous recombination in *Escherichia coli*. *Nat Biotechnol* **18:** 1314–1317

Zimmer M, Palmer A, Kohler J, Klein R (2003) EphB-ephrinB bi-directional endocytosis terminates adhesion allowing contact mediated repulsion. *Nat Cell Biol* **5:** 869–878